Influence of Meteorological Balloons on Temperature Measurements with Radiosondes: Nighttime Cooling and Daylight Heating

HELMUT K. E. TIEFENAU

Albin Sprenger KG GmbH and Company, Harz, Federal Republic of Germany

ALFONS GEBBEKEN

E 91 Army of the Federal Republic of Germany, Meppen, Federal Republic of Germany

(Manuscript received 10 July 1987, in final form 4 April 1988)

ABSTRACT

Temperatures measured by radiosondes ascending on free-flying balloons within middle latitudes above the troposphere differ significantly from measurements made with the same radiosondes descending on parachutes after the balloons have burst. During ascending flights, values measured below the balloons are too low for night ascents, and too high for daylight ascents. The divergences grow with decreasing air pressure. During night ascents, the adiabatic gas temperature decreases within the balloon, lowering the balloon skin temperature. During daylight ascents, in contrast, solar radiation heats the balloon skin, superimposing a heating effect upon the adiabatic cooling effect on the balloon skin. In each case the resulting surface temperature of the balloon affects via heat exchange the airstream passing the balloon. Both effects grow with increasing height. Temperature diffusion velocity calculations show a very long stability of the wake. Since the radiosonde sensor will measure mainly the temperature within the balloon wake, the aforementioned influences cannot be neglected, if true temperature measurements are the aim.

1. Introduction

In the course of tests on a new generation of radiosondes designated for use in the weather service of the West German Army, temperature profiles of balloon-borne radiosondes were compared with temperature measurements of these sondes during parachute-borne descents. The results were not identical. Research into this discrepancy revealed two effects: The first is an air cooling effect. A balloon expands during ascent. Its inside pressure is always nearly the same as the outside pressure. This expansion would result in an adiabatic cooling of the balloon gas. However, due to energy transfer from the air passing the balloon skin, the temperature of the balloon gas remains close to the outside temperature, cooling down the air passing by. This effect mainly gains importance above the tropopause, where the temperature profile is almost isothermal. It can be clearly demonstrated in night ascents. The second effect is a heating effect. During daylight ascent, the balloon skin is heated by the sun's radiation. Though this effect is qualified by the adiabatic cooling, it can be depicted separately if the nighttime cooling is measured first.

Corresponding author address: Dr. H. Tiefenau, Albin Sprenger KG GmbH and Co., Postfach 20, D-3424 St. Andreasberg/Harz, Federal Republic of Germany.

Both cooling and heating effects influence the balloon wake temperature. The balloon wake diameter, as well as the temperature changes induced by the cooling and heating effects, can be described by a mathematical model. Both the temperature and the diameter of the balloon wake depend on the gain in altitude of the instrument. The air layer thickness around the balloon, within which the heat exchange takes place, can be calculated by measuring the temperature change rate at a certain level (here 10 hPa). Applying this to the current model allows the wake diameter to be determined for the complete ascent, with only a small error margin. Calculating the heat flux from the balloon wake as a function of time reveals that the heating and cooling effects cannot be neglected, even when there is a very great distance between the balloon and the radiosonde. Typical temperature microstructures measured 30 m below the balloon give evidence of different behavior in night and day ascent conditions. Examples of this follow.

2. The radiosondes used

In 1982, after thorough tests, the West German Army introduced a new generation of radiosondes. These sondes transmit a complete set of measurements every second, enabling analysis of atmospheric fine structures. This generation of radiosondes consists of three types: (i) Temperature sondes for heights up to

10 km without solar radiation shielding. (ii) Temperature and humidity sondes for heights up to 20 km with solar-radiation-shielded sensors. (iii) Temperature, humidity and air pressure sondes for heights up to 40 km or more, shielded against direct and reflected solar radiation.

The temperature accuracy of all sondes is better than 0.2 K for temperatures between +50 and −90 degrees C. The time constant of the temperature sensor at 5 m s^{-1} air velocity is less than one second for 90% response to a temperature step. Radiation shielding is accomplished by a square polyfoam tube, 12 mm thick, 65 mm edge length and 235 mm high. The temperature sensor is protected against rain and vertical radiation. A bead thermistor of 0.7 mm diameter coated with waterproof and radiation-reflective lacquer is used as a sensor. All experiments described here were performed with the abovementioned three-parameter sondes and 1000 g balloons of various manufacturers such as Everts, Kaysam and Totex.

3. Cooling effect during night ascents

During a balloon ascent, the gas inside the balloon expands adiabatically if there is no heat exchange with the surrounding air. Consequently, the balloon gas cools down. Depending on the balloon type, the pressure inside will exceed the surrounding air pressure by approximately 1–2 hPa.

This decrease in the temperature of the balloon gas has almost no influence within the troposphere, where the natural temperature gradient is almost adiabatic. Above the troposphere, conditions alter. The surrounding temperature is nearly isothermal, whilst the balloon continues to cool down adiabatically. With c_p (H_2) = 14.269 W s g^{-1} K^{-1} and a weight of 90 g for one standard cubic meter of hydrogen (i.e., 3.5 × 90 g for the balloon used), the balloon will absorb 4.495 W s^{-1} during adiabatic energy loss of 1 K and succeeding adaptation to the isothermal condition. This heat amount is supplied by the air streaming past the balloon, resulting in lower air temperature of the wake. The calculated and observed values listed in Tables 1 and 2 are based on a 3.5 standard cubic meter hydrogen-filled balloon at a mean ascent velocity of 5.5 m s^{-1} and on c_p (air) = 1.009 W s g^{-1} K^{-1} at −60°C; c_p (H_2) and c_p (air) are not temperature-dependent between 100 K and 800 K (Becker 1966) and are thus constant within the temperature range of interest here. Simultaneous measurements of internal balloon temperature and the surrounding air temperature during night ascents show an inferior temperature of −9 K inside the balloon at 13 km height. This difference grows to approximately −18 K at a height of 28 km. The adiabatic temperature difference between heights of 13 and 28 km amounts to 342 K at −60°C air temperature (Becker 1966). Consequently, an isothermal condition inside the balloon is assumed for the calculation of energy absorbed by the balloon gas. This leads to an error of $^9/_{342}$ = 2.6%, which may be neglected.

TABLE 1.

A (hPa)	B (m^3)	C (m)	D (m^2)	E (m^3)	F (m)	G (m^2)
300	8.33	1.25	4.96	9.56	1.32	5.45
200	12.46	1.44	6.51	14.30	1.51	7.12
100	24.73	1.81	10.26	28.39	1.89	11.25
90	27.44	1.87	11.00	31.49	1.96	12.06
80	30.80	1.94	11.88	35.36	2.04	13.02
70	35.11	2.03	12.96	40.30	2.13	14.21
60	40.82	2.14	14.33	46.86	2.24	15.71
50	48.75	2.27	16.13	55.95	2.37	17.69
40	60.50	2.44	18.63	69.44	2.55	20.43
30	79.70	2.67	22.39	91.48	2.80	24.61
25	94.74	2.83	25.13	108.74	2.96	27.54
20	116.77	3.03	28.88	134.03	3.17	31.66
18	128.75	3.13	30.83	147.77	3.28	33.79
16	143.46	3.25	33.12	164.66	3.40	36.32
14	161.97	3.38	35.92	185.91	3.54	39.38
12	185.97	3.54	39.39	213.45	3.71	43.21
10	218.31	3.74	43.83	250.58	3.91	48.05
9	239.10	3.85	46.57	274.44	4.03	51.06
8	264.27	3.98	49.79	303.33	4.17	54.58
7	295.36	4.13	53.62	339.01	4.33	58.78
6	334.75	4.31	58.29	384.22	4.51	63.90

Note: A = pressure level; B = balloon volume, filled at 1000 hPa and 10°C with 3.5 m^3 in respect to inside temperature of −70°C and 1.5 hPa inside overpressure (night condition); C = resulting balloon radius (night condition); D = resulting cross-sectional balloon area (night condition); E = like B, but with inside temperature of −40°C (daylight condition); F = resulting balloon radius (daylight condition); G = resulting balloon cross-sectional area (daylight condition).

The dry adiabatics are calculated from $\theta = T(1000/P(x))^{0.286}$ and $P(x) = P_0 \cdot e^{-mg \times k^{-1} T^{-1}}$, where θ = potential temperature, $P(x)$ = pressure, P_0 = 225 hPa at 11 km height, x = height, m = molecular mass of air, g = 9.81 m s^{-2}, k = $1.3806 \cdot 10^{-23}$ W s K^{-1} and T = 213 K. (See Table 1.) The considerable amount of energy transferred because of adiabatic expansion must lead to heat loss within the air streaming past the balloon. This cooling effect was first observed during a measuring period in August 1979. For a period of one week, all data from radiosonde flights carried out at midnight were registered during both balloon-borne ascents and parachute-borne descents. The observed effect of lower temperature readings during ascents than during descents was verified in the years following, whenever data from ascents and descents during night flights were available. The following calculations are based on the values obtained during night ascents, in order to exclude the influence of solar radiation on the balloon surface. The measured values in Table 2 (K) are based on 25 ascents.

First, the difference in potential temperature per meter height was calculated at −60°C, as was this difference per second at an ascent velocity of 5.5 m s^{-1}. From these results, the energy flow into a 3.5 cubic

TABLE 2.

A (hPa)	H (km^{-1})	I ($K\ s^{-1}$)	J (kW)	K (K)	L ($m^3\ s^{-1}$)	M (m^2)
300	0.0138	0.0761	0.34	−0.1 ± 0.8	6.93	1.26
200	0.0155	0.0855	0.38	−0.1 ± 0.8	11.67	2.12
100	0.0189	0.1042	0.47	−0.2 ± 0.7	14.22	2.59
90	0.0195	0.1074	0.48	−0.2 ± 0.7	16.29	2.96
80	0.0202	0.1111	0.50	−0.3 ± 0.7	12.63	2.30
70	0.0210	0.1154	0.52	−0.4 ± 0.6	11.25	2.05
60	0.0219	0.1206	0.54	−0.5 ± 0.9	10.97	2.00
50	0.0231	0.1270	0.57	−0.7 ± 0.9	9.91	1.80
40	0.0246	0.1354	0.61	−0.9 ± 0.7	10.27	1.87
30	0.0267	0.1470	0.66	−1.2 ± 0.5	11.15	2.03
25	0.0282	0.1549	0.70	−1.5 ± 0.9	11.28	2.05
20	0.0300	0.1651	0.74	−1.8 ± 1.0	12.52	2.28
18	0.0309	0.1702	0.76	−2.0 ± 1.4	12.90	2.35
16	0.0320	0.1760	0.79	−2.2 ± 1.4	13.65	2.48
14	0.0332	0.1828	0.82	−2.5 ± 1.9	14.26	2.59
12	0.0347	0.1911	0.86	−2.8 ± 1.9	15.52	2.82
10	*** 0.0366	*** 0.2013	*** 0.90	*** −3.3 ± 1.9	*** 16.65	*** 3.03
9	0.0377	0.2075	0.93	−3.9 ± 2.0	16.14	2.93
8	0.0390	0.2146	0.96	−4.6 ± 2.2	15.92	2.89
7	0.0405	0.2229	1.00	−5.4 ± 2.3	16.10	2.93
6	0.0424	0.2330	1.05	−6.5 ± 2.5	16.31	2.97

Note: A = pressure level; H = gradient of potential temperature at −60°C in km^{-1}; I = gradient of potential temperature at −60°C in km^{-1} at 5.5 m s^{-1}; J = energy flow into balloon filled with 3.5 standard m^3 hydrogen; K = measured temperature drop inside the wake and standard deviation; L = wake volume flow, calculated from J and K; M = wake cross-sectional area, calculated from L at 5.5 m s^{-1}.

meter hydrogen-filled balloon was calculated, which is necessary to maintain the isothermal condition. This value and the measured temperature differences allow us to calculate the wake volume flow (constant temperature) and the wake cross-sectional area. The calculated values are listed in Table 2. If we assume that the heat-exchange layer on the balloon surface is of constant thickness, independent of the actual air pressure, there is a linear correlation between balloon diameter and wake surface of intersection. The wake cross-sectional area was adapted to the 10 hPa-level and calculated as described here (see Tables 2, 3, and 4). From the (known) balloon circumference and the wake cross-sectional area, calculated for the 10 hPa-level, the linear correlation between balloon circumference and wake diameter was used to calculate the wake diameters for all other pressure levels (see Tables 2, 3 and 4).

The heat-exchange-layer thickness d at the balloon equator, e.g., within the 10 hPa-level from balloon radius r = 3, 74 m and wake surface A = 3, 03 square meters, yields:

$$d = A/2\pi r \quad d = 12.9 \text{ cm}.$$

This means that there is a heat exchange layer around the balloon equator with a horizontal thickness of d = 12.9 cm. All elements within this layer have an average temperature (listed in Table 2) and mix to this average temperature evenly within the balloon wake. For Reynold numbers smaller than 10^5, the thickness of the heat exchange layer will increase with decreasing pressure, where $d \approx (\sqrt{P})^{-1}$, ($P$ = air pressure). Reynold numbers of more than 10^5 to 10^6 produce a wake with a vortex structure. Such a vortex is very stable, and heat exchange with the surrounding air is accom-

TABLE 3.

A (hPa)	N (m^2)	O ($m^3\ s^{-1}$)	P ($kg\ s^{-1}$)	Q (K)
300	0.18	0.297	0.491	0.69
200	0.25	0.275	0.455	0.84
100	0.44	0.242	0.400	1.01
90	0.49	0.243	0.402	1.02
80	0.54	0.238	0.394	1.28
70	0.60	0.231	0.382	1.37
60	0.68	0.224	0.371	1.47
50	0.79	0.217	0.359	1.60
40	0.95	0.209	0.346	1.78
30	1.21	0.200	0.330	2.02
25	1.41	0.194	0.321	2.20
20	1.70	0.187	0.309	2.42
18	1.86	0.184	0.304	2.52
16	2.05	0.180	0.298	2.67
14	2.29	0.176	0.292	2.83
12	2.60	0.172	0.284	3.06
10	*** 3.03	*** 0.167	*** 0.276	*** 3.29
9	3.31	0.164	0.271	3.46
8	3.65	0.161	0.166	3.64
7	4.08	0.157	0.260	3.88
6	4.64	0.153	0.253	4.19

Note: A = pressure level; N = wake cross-sectional area, calculated from exchange layer $d \approx (\sqrt{P})^{-1}$ and adapted at 10 hPa; Q = wake volume airstream in standard $m^3\ s^{-1}$; P = wake air mass stream in $kg\ s^{-1}$; Q = calculated temperature drop from J and P.

plished by normal diffusion as shown in section 5. Furthermore, a vortex structure yields a nearly rectangular temperature profile across the wake, as assumed in the calculations. However, we are just in the range of Reynold numbers which include a step from laminar to turbulent airflow. Therefore, it is not possible to calculate exactly the wake area, due to its physical conditions (see approach with $d \approx (\sqrt{P})^{-1}$ in Table 3).

The assumption that cross-sectional area and balloon radius are linearly correlated is corroborated by the very close relationship between measured and calculated temperature drop inside the wake (see Table 4). Therefore, this model is used as a first approximation for further calculations in this paper. This is the precondition for starting out with a rectangular temperature distribution, as assumed in section 5. To accept a bell-shaped temperature distribution curve directly beneath the balloon (as shown in Fig. 1) would mean only a slight time lag in the diffusion characteristics of the balloon wake. For the other pressure layers the temperature drop was calculated from the known flux and the calculated cross-sectional area. The measured and calculated values are indicated in Table 4.

The agreement of measured and calculated values can be considered good, since calculations were made under slightly simplified conditions and measured values at pressures below 10 hPa are based on low incidence and thus have no statistical significance. Furthermore, the pressure difference between the inner and outer sides of the balloon becomes significant at very low pressures. A pressure difference of 1.5 hPa was used for calculations of the balloon volume in Table 1.

4. Heating effect during daylight ascents

The existence of a heating effect during daylight ascents has been recognized for more than 40 years. This effect was studied in detail using data from 27 ascents between January 1983 and October 1984 and also verified by later measurements, as listed in Table 5a, (column 2). Analysis of these measurements leads to the results discussed here. The previously described cooling effects obtain for daylight ascents as well. For the calculation of daylight effects, the influence of higher balloon-gas temperature on balloon volume, as well as on cooling of the wake cross-sectional area, was considered (see Table 1). If, in spite of the presence of the air-cooling effect, a heating effect is observed, it will be due mainly to radiation absorption by the balloon. Heating of the temperature sensor by direct or reflected solar radiation, as well as deficient sensor ventilation, may be excluded. Ney et al. (1961) demonstrate that the ventilation of sensors at pressures far below 10 hPa is of minor importance.

A funnel on top of the radiation shielding tunnel for the increase of airspeed at the temperature sensor is of no use (Ney et al. 1961). It may even distort humidity measurements if precipitation/snow remains on its surface. Consequently, the upper cloud surface cannot be distinguished. It is assumed that the energy absorbed from solar radiation (1.3 kW m^{-2}) is proportional to

TABLE 4.

A (hPa)	$\bar{N}$ (m^2)	$\bar{O}$ ($m^3 s^{-1}$)	$\bar{P}$ (kg s^{-1})	$\bar{Q}$ (K)	K (K)	R (K)
300	1.01	1.667	2.756	−0.12	−0.1	−0.02
200	1.17	1.287	2.128	−0.18	−0.2	−0.08
100	1.47	0.809	1.338	−0.35	−0.2	−0.15
90	1.51	0.747	1.235	−0.39	−0.2	−0.19
80	1.57	0.691	1.142	−0.44	−0.3	−0.14
70	1.64	0.631	1.043	−0.50	−0.4	−0.10
60	1.73	0.571	0.944	−0.58	−0.5	−0.08
50	1.84	0.506	0.837	−0.69	−0.7	−0.01
40	1.98	0.436	0.721	−0.85	−0.9	+0.05
30	2.16	0.356	0.589	−1.13	−1.2	+0.07
25	2.29	0.315	0.521	−1.36	−1.5	+0.14
20	2.45	0.270	0.446	−1.67	−1.8	+0.13
18	2.54	0.251	0.415	−1.85	−2.0	+0.15
16	2.63	0.231	0.382	−2.09	−2.2	+0.11
14	2.74	0.211	0.347	−2.38	−2.5	+0.14
12	2.87	0.189	0.312	−2.78	−2.8	+0.02
10 **	3.03 **	0.167 **	0.276 ***	−3.29 **	−3.3 **	+0.01
9	3.12	0.154	0.255	−3.68	−3.9	+0.22
8	3.22	0.142	0.235	−4.12	−4.6	+0.48
7	3.35	0.129	0.213	−4.74	−5.4	+0.66
6	3.49	0.155	0.190	−5.58	−6.5	+0.92

Note: A = pressure level; $\bar{N}$ = wake cross-sectional area, calculated with constant thickness of exchange layer and adapted at 10 hPa; $\bar{O}$ = wake volume air stream in standard $m^3 s^{-1}$; $\bar{P}$ = wake air mass flow in kg s^{-1}; $\bar{Q}$ = calculated temperature drop from I and $\bar{P}$; K = measured temperature drop inside the wake; R = difference $\bar{Q} - K$.

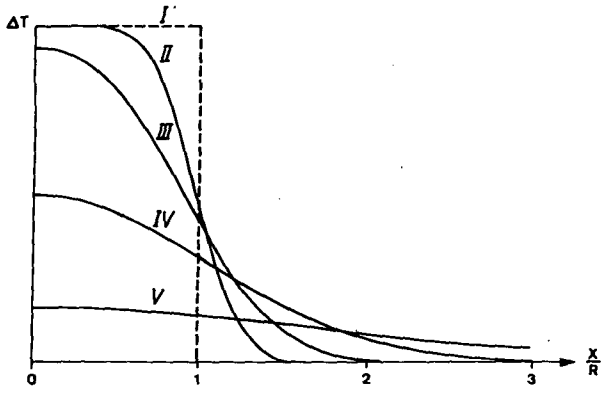

FIG. 1. Temperature profiles as function of the distance from the central z-line in units of the wake radius for five different times.

the balloon surface exposed to the sun. The measured difference between night cooling and daylight heating was used to calculate the absorbed radiation performance for the 10 hPa level by pursuing the same procedure as for night cooling. The result was a value of 45.9 W m^{-2}. This is 3.53% of the total radiation. The resulting wake heating effect is given in Table 5. The difference between measured and calculated heating is less than 1.3 K, indicating that the premises were correct as a first approximation. Trend variations may be rooted in reflection/absorption properties of the balloon skin. It must be assumed that absorption drops with decreasing skin thickness resp. diminishing outer pressure. The result would be a closer approximation to the measured values.

5. Approach to diffusion

When temperature is measured with a radiosonde suspended beneath a balloon, it is of interest to know how fast a temperature rise or drop diffuses perpendicular to the wake.

The general equation for diffusion is:

$$\frac{\partial T}{\partial t} = \lambda_T \Delta T, \tag{1}$$

where T is the temperature rise/drop, Δ the Laplacian operator, and λ_T the thermal conductivity, which is assumed to be constant. We assume that T and z are independent. The two-dimensional temperature distribution after heating up the point x_0, y_0 in the x–y plane is described by

$$T = (\text{const.})\,\frac{1}{t}\,e^{-\{[(x-x_0)^2+(y-y_0)^2]/4\lambda_T t\}}. \tag{2}$$

The extension to an initially heated surface yields:

$$T(x, y, t) = \frac{1}{4\pi\lambda_T t}\iint T_0(\xi, \eta)e^{-\{[(x-\xi)+(y-\eta)^2]/4\lambda_T t\}}\,d\xi d\eta, \tag{3}$$

TABLE 5a.

A (hPa)		S (K)	K (K)		$\bar{K}$ (K)		T (K)		U (m^3 s^{-1})
300		—	—		—		—		1.744
200		—	—		—		—		1.347
100		+0.2 ± 1.0	−0.2		−0.2		+0.4		0.843
90		+0.2 ± 1.0	−0.2		−0.2		+0.4		0.782
80		+0.3 ± 1.0	−0.3		−0.3		+0.6		0.723
70		+0.5 ± 1.0	−0.4		−0.4		+0.9		0.660
60		+0.7 ± 1.0	−0.5		−0.5		+1.2		0.597
50		+1.0 ± 0.9	−0.7		−0.7		+1.7		0.529
40		+1.3 ± 1.4	−0.9		−0.9		+2.2		0.456
30		+1.8 ± 1.4	−1.2		−1.1		+2.9		0.373
25		+2.1 ± 1.8	−1.5		−1.4		+3.5		0.330
20		+2.6 ± 2.2	−1.8		−1.7		+4.3		0.283
18		+2.8 ± 2.0	−2.0		−1.9		+4.7		0.263
16		+3.0 ± 2.0	−2.2		−2.1		+5.1		0.242
14		+3.3 ± 2.2	−2.5		−2.4		+5.7		0.221
12		+3.8 ± 2.2	−2.8		−2.7		+6.5		0.198
10	***	+4.5 ± 2.2	−3.3	***	−3.2	***	+7.7	***	0.175
9		+4.9 ± 2.3	−3.9		−3.7		+8.6		0.161
8		+5.4 ± 2.4	−4.6		−4.4		+9.8		0.149
7		+6.3 ± 2.5	−5.4		−5.2		+11.5		0.135
6		+8.0 ± 2.7	−6.5		−6.3		+14.3		0.120

Note: A = pressure level; S = measured heating 30 m below balloon at daytime with standard deviation; K = measured cooling 30 m below balloon at night; $\bar{K}$ = cooling adapted to daylight condition according to C and F; T = resulting heating ($S - \bar{K}$); U = wake volume stream adapted from $\bar{O}$ to daylight condition; V = wake air mass stream; W = necessary energy absorption, calculated from T and V at −60°C; X = absorbed energy in W m^{-2}, calculated from W and G ($X = W/G$); Y = temperature drop, calculated from V and X, adapted to W at 10 hPa; Z = temperature difference ($T - Y$).

TABLE 5b.

A (hPa)	V ($m^3 s^{-1}$)	W (kW)	X (kW m^{-2})	Y (K)	Z (K)
300	2.883	—	—	—	—
200	2.227	—	—	—	—
100	1.394	0.553	0.516	0.37	0.13
90	1.293	0.512	0.516	0.40	0.00
80	1.195	0.711	0.578	0.49	0.11
70	1.091	0.973	0.597	0.55	0.35
60	0.987	1.174	0.721	0.74	0.94
50	0.875	1.474	0.812	0.94	0.76
40	0.754	1.644	0.937	1.25	0.95
30	0.617	1.773	1.129	1.85	1.05
25	0.546	1.894	1.264	2.34	1.16
20	0.468	1.994	1.453	3.13	1.17
18	0.435	2.026	1.551	3.60	1.10
16	0.400	2.021	1.667	4.21	0.89
14	0.365	2.061	1.807	5.00	0.70
12	0.327	2.107	1.983	6.12	0.38
10 **	0.289 **	2.205 **	2.205 **	7.70 **	0.00
9	0.266	2.267	2.343	8.89	−0.29
8	0.246	2.389	2.505	10.28	−0.48
7	0.223	2.542	2.697	12.20	−0.70
6	0.198	2.806	2.932	14.94	−0.64

See Note on Table 5a.

where $\lim_{t\to 0} T(x, y, t) = T_0(x, y)$ is given in the temperature distribution for $t = 0$.

For our evaluation let $T_0(x, y) = T_0$ = constant for $x^2 + y^2 \leq R^2$, else $T_0(x, y) = 0$. The temporal variation for $x, y = 0$ can be found by elementary integration. Then

$$T(0, 0, t) = T_0(1 - e^{-(R^2/4\lambda_T t)}) \qquad (4)$$

with $t_{1/2} = \dfrac{R^2}{4\lambda_T \ln 2}$ = half-life period τ.

For $x, y \neq 0$ $T(x, y, t)$ was computed numerically. The development of the initially constant temperature distribution within an infinite cylinder is shown in Fig. 1.

The thermal conductivity is given by

$$\lambda_T = \frac{\lambda}{\rho c_p}$$

where λ = heat conductivity, ρ = mass density, and c_p = thermal capacity (constant pressure). With $\lambda = 0.0241$ J s^{-1} m^{-1} K^{-1}, $c_p = 29.13$ J Mol^{-1} K^{-1}, $\rho = 1.29$ kg m^{-3} and

$$\lambda_T = \lambda_{T_0} \frac{T^2}{T_0^2} \times \frac{P_0}{P} \quad \text{at } -60°C \qquad (5)$$

follows:

$$t_{1/2} = R^2(3.3 \times 10^4) \frac{P}{P_0}. \qquad (6)$$

This proves, as shown in Table 2, for 100 hPa at −60°C and wake radius 0.72 m, halving of temperature after 1723 s = 28 min. Accordingly, at 10 hPa and wake radius 1.06 m after 372 s = 6.2 min. Obviously, the too cold/warm wake has a very stable shape which remains steady at an ascent rate of 5.5 m s^{-1} and undergoes no significant configuration changes even up to 30 m beneath the balloon. The only advantage of a long tether between the balloon and the sonde is the fact that because the sonde is swung out of the wake influence for a considerable amount of time, an average temperature measurement based on a sufficiently long-time data sample shifts closer to true air temperature.

6. The temperature wake and its effect on *T*-measurements

During night ascent, the cooling effect under the balloon occurs symmetrically with respect to the vertical balloon axle. The usual tether length between balloon and sonde is approximately 30 m. Generally, the sonde swings beneath the balloon. These oscillations can take the form of linear, elliptical or circular motion. In the case of circular movements, the sonde will remain either at the wake circumference or outside of the temperature wake area with large circular movements. According to Table 4 ($\bar{N}$), the wake cross-sectional area is 1.47 m^2 at 100 hPa and 3.03 m^2 at 10 hPa.

The oscillation time of a 30 m pendulum is calculated as follows:

$$t = 2\pi \sqrt{\frac{1}{g}} = 2\pi \sqrt{\frac{30 \text{ m}}{9.8 \text{ m} \cdot \text{s}^{-2}}} = 11 \text{ s}. \qquad (7)$$

Therefore, we expect variations of the measured temperature during night ascents with lapse terms of approximately 5.5 s. Such temperature readings with a sine wave resembling character in fact occur in undeterminable sequences. This sine wave is actually a right-angle wave produced when the sensor crosses the wake; the smoothed edges are an artifact caused by the sensor's time delay (approximately 1 s).

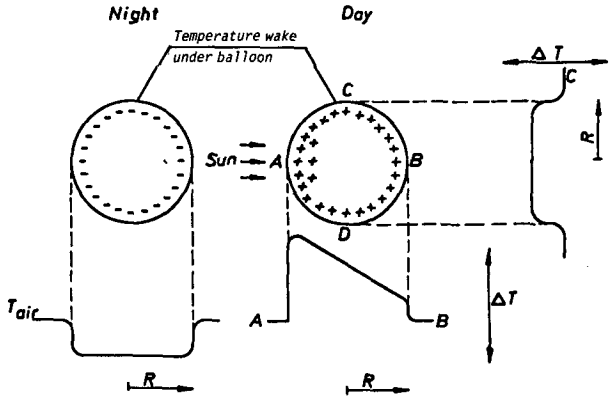

FIG. 2. Temperature distribution below a balloon during night and day ascents.

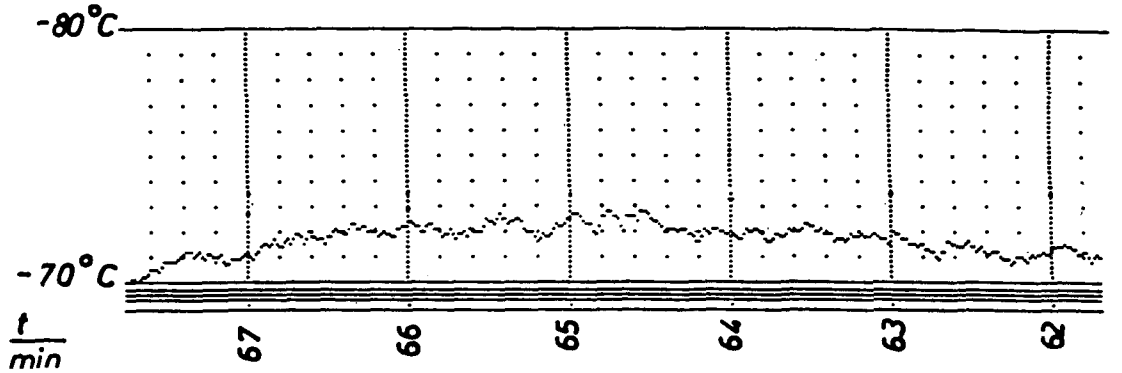

FIG. 3. Typical fine-structure temperature registration during a day ascent.

During daytime ascents, the picture is somewhat more intricate. The symmetrical cooling is qualified by unilateral heating due to solar radiation. Most of the nonabsorbed radiation is reflected (the rationale for using white balloons). Radiation absorption on the shade side of the balloon can probably be neglected.

Oscillatory movements of the sonde—whether circular, elliptic or linear—mean a constant change between warm and cold, except for movements perpendicular to solar radiation. For this reason, we find period durations of 5.5 s as well as 11 s. As expected, the temperature oscillation amplitude with 11 s period is twice the width of one with a period duration of 5.5 s.

Figure 2 shows the expected temperature distribution below a balloon during day and night ascents. Figure 3 shows typical examples for oscillations within the temperature record during a day ascent, including periods of approximately 5.5 s and 11 s, as well in change as superimposed ones.

7. Discussion

The wake diameter was calculated for laminar or vortex stream. Turbulence effects might accelerate the drift-off from the "temperature wake." The measured temperature drops and rises were measured as mean values—at a distance of 30 m from the balloon—in comparison to measurements made during the descent of a parachute-borne radiosonde.

Since the amplitudes of the temperature oscillations measured below the balloon are more narrow than the calculated cooling and heating, it may be assumed—considering the quick response of the temperature sensor—that the temperature wake drifts apart quicker than described in the model presented here. This means that the sonde mostly swings within the wake and can only register changes remaining at a distance of 30 m, corresponding to approximately 5.5 s from the balloon. This would explain why the calculated temperature changes, compared with the surrounding air, rise somewhat faster with gained height than the measured ones.

8. Conclusions

Measurements made in heights above 30 km are based on a few random tests and are thus less reliable. The radiosonde system used has an error tolerance of less than ±0.2 K.

Further test series, including ones with small balloons, should be performed in order to substantiate or correct the reported results.

When balloons with less volume are used, the wake temperature difference will diminish during night ascents, since the volume will increase the wake cross-sectional area in the relation $\frac{\text{volume}}{\text{cross-sectional area}} = \frac{r^3}{r^2}$. During daylight ascents, the heating of the wake of smaller balloons will increase, since balloon surface and wake cross-sectional area are proportional, while superimposed cooling is lower.

A feasible way to measure air temperature correctly is to place the temperature sensor on top of the balloon. However, this would make balloons and sondes more expensive and would complicate handling in routine use.

Acknowledgments. We expressly thank Dr. Klaus Richter of the "MPI für Aeronomie," D 3411 Lindau a. Harz, FRG, for his kind assistance in compiling the two-dimensional diffusion model and the numerical integration of the temperature profiles.

REFERENCES

Becker, R., 1966: *Theorie der Wärme.* Springer Verlag, 10, 81 ff.

Ney E. P., R. W. Maas and W. F. Huck, 1961: The measurement of atmospheric temperature. *J. Meteor.*, **18**, 60–80.